Density driven flow in uncertain fractured porous media via MLMC

Alexander Litvinenko[2][0000−0001−5427−3598], Dmitry Logashenko[1][0000−0001−9384−5296], Raul Tempone[1,2], and Gabriel Wittum[1]

[1] King Abdullah University of Science and Technology, Thuwal, Saudi Arabia
{dmitry.logashenko,raul.tempone,gabriel.wittum}@kaust.edu.sa
[2] Department of Mathematics, RWTH Aachen, Aachen, Germany
litvinenko@uq.rwth-aachen.de

Abstract. We consider a Henry-like intrusion problem, where fluid flow is driven by variations in fluid density. The Multi-Level Monte Carlo (MLMC) method is employed to estimate the mean value of a quantity of interest (QoI). The QoI is defined as the earliest time at which the mass fraction of salt exceeds a given threshold.
In our setting, porosity, permeability, recharge, and fracture thickness are treated as uncertain parameters and modeled as random variables. For each realization of these parameters, the evolution of the salt mass fraction is governed by a system of nonlinear, time-dependent partial differential equations (PDEs). We demonstrate that the MLMC method can be effectively applied to this problem, significantly reducing computational costs compared to classical Monte Carlo methods.
The findings of this study have the potential to enhance and accelerate the monitoring of drinking water resources and pollution dynamics.

Keywords: density driven flow · uncertainty quantification · Multi Level Monte Carlo · geometric multigrid method

1 Introduction

Uncertainty in geological parameters, such as porosity, permeability, and fracture characteristics, poses significant challenges to accurate prediction of aquifer behavior, especially in the context of seawater intrusion and freshwater management. This is especially important for fractures, which introduce strong anisotropy into flow and transport phenomena, further complicating the modeling process. Real aquifers inherently exhibit uncertain fracture characteristics, making their accurate representation highly complex.

As demonstrated in [9], combining the Multi-Level Monte Carlo (MLMC) method with the geometric multigrid method (GMG) is a highly effective strategy for addressing complex flow problems. Related studies, such as [6] and [7], explored the use of Polynomial Chaos Expansion (PCE) in the Elder problem, another density-driven flow challenge. In our previous work [10], we successfully applied the coupled GMG and MLMC methods to a problem involving

fractures. This paper builds upon those results, considers another quantity of interest (QoI) and extends the methodology and findings. For a comprehensive review of the relevant literature and detailed descriptions of the problem settings and methods, we refer to [10]. Here, we adopt the benchmark model from [4], a generalization of the classic Henry problem [5], a standard test case for density-driven groundwater flow solvers [13, 2].

Novelty. We analyze the performance of the MLMC method for a challenging density-driven flow problem governed by coupled, nonlinear system of PDEs with discontinuous behavior. By combining MLMC with GMG solvers, we estimate the mean of the time at which the salt mass fraction exceeds a specified threshold. Our results show that MLMC can achieve speedups of up to 1000x compared to standard Monte Carlo methods. The uncertainties considered include spatially variable porosity, time-dependent recharge, and fracture aperture.

2 Modeling

We consider density-driven flow in a fractured, immobile, fully saturated porous medium. The liquid phase consists of a salt solution with a variable salt mass fraction. Our model follows the approach of [11], to which we refer for further details. The fracture, with a physical aperture of ϵ, is represented as a lower-dimensional manifold. We assume that the fractures remain fixed and denote the entire aquifer domain by $\mathcal{D} \subseteq \mathbb{R}^d$, with the fracture surface $\mathscr{S} \subset \mathcal{D}$ and the surrounding matrix $\mathscr{M} \subseteq \mathcal{D}$, such that $\overline{\mathscr{M}} \cup \overline{\mathscr{S}} = \overline{\mathcal{D}}$. The porosity and permeability of the matrix are denoted by ϕ_m and $\mathbf{K}_m$, respectively, while those of the fracture are ϕ_f and K_f. Then the flow and transport in each of these subdomains are described by the mass conservation laws

$$\left.\begin{aligned} &\partial_t(\phi_m \rho_m) + \nabla \cdot (\rho_m \mathbf{q}_m) = 0 \\ &\partial_t(\phi_m \rho_m c_m) + \nabla \cdot (\rho_m c_m \mathbf{q}_m - \rho_m \mathbf{D}_m \nabla c_m) = 0 \end{aligned}\right\} \quad x \in \mathscr{M} \quad \text{and} \tag{1}$$

$$\left.\begin{aligned} &\partial_t(\phi_f \epsilon \rho_f) + \nabla^{\mathscr{S}} \cdot (\epsilon \rho_f \mathbf{q}_f) + Q_{fn}^{(1)} + Q_{fn}^{(2)} = 0 \\ &\partial_t(\phi_f \epsilon \rho_f c_f) + \nabla^{\mathscr{S}} \cdot (\epsilon \rho_f c_f \mathbf{q}_f - \epsilon \rho_f D_f \nabla^{\mathscr{S}} c_f) + P_{fn}^{(1)} + P_{fn}^{(2)} = 0 \end{aligned}\right\} \quad x \in \mathscr{S}, \tag{2}$$

where c_m, c_f, $\rho_m = \rho(c_m)$, $\rho_f = \rho(c_f)$ are salt mass fractions and densities of the fluid phase in $\mathscr{M}$ and $\mathscr{S}$, and $\mathbf{D}_m$, D_f are the diffusion-dispersion coefficients in these media. For the flow velocities $\mathbf{q}_{m,f}$, we assume the Darcy's laws:

$$\mathbf{q}_m = -\tfrac{\mathbf{K}_m}{\mu}(\nabla p_m - \rho_m \mathbf{g}), \qquad x \in \mathscr{M}, \tag{3}$$

$$\mathbf{q}_f = -\tfrac{K_f}{\mu}(\nabla^{\mathscr{S}} p_f - \rho_f \mathbf{g}), \qquad x \in \mathscr{S}, \tag{4}$$

where $p_{m,f}$ are pressure fields, μ viscosity of the fluid phase, $\mathbf{g}$ the gravity.

To model the mass exchange between $\mathscr{M}$ and the fracture, we distinguish between two sides of $\mathscr{S}$, namely $\mathscr{S}^{(1)}$ and $\mathscr{S}^{(2)}$, coinciding with $\mathscr{S}$ in position, but being interfaces between the fracture and $\mathscr{M}$ with outer normals $\mathbf{n}^{(1)}$ and $\mathbf{n}^{(2)} = -\mathbf{n}^{(1)}$. On $\mathscr{S}^{(k)}$, we assume mass fractions $c_m^{(k)}$ and pressures $p_m^{(k)}$, so

that these fields are discontinous on $\mathscr{S}$. The mass fluxes of the liquid phase and the salt through $\mathscr{S}^{(k)}$ are denoted by $Q_{fn}^{(k)}$ and $P_{fn}^{(k)}$:

$$\left.\begin{aligned} Q_{fn}^{(k)} &:= \rho(c_m^{(k)}) q_{fn}^{(k)} \\ P_{fn}^{(k)} &:= \rho(c_m^{(k)}) c_{\text{upwind}}^{(k)} q_{fn}^{(k)} - \rho(c_m^{(k)}) D_{fn}^{(k)} \frac{c_m^{(k)} - c_f}{\epsilon/2} \end{aligned}\right\} \quad x \in \mathscr{S}^{(k)}, \quad \text{with} \tag{5}$$

$$q_{fn}^{(k)} := -\frac{K_{fn}^{(k)}}{\mu}\left[\frac{p_m^{(k)} - p_f}{\epsilon/2} - (\rho(c_m^{(k)}) - \rho_f)\mathbf{g}\cdot\mathbf{n}^{(k)}\right], \qquad x \in \mathscr{S}^{(k)}, \tag{6}$$

where $K_{fn}^{(k)}$ is the normal permeability and $D_{fn}^{(k)}$ the normal effective diffusion-dispersion coefficient at $\mathscr{S}^{(k)}$, $c_{\text{upwind}}^{(k)}$ is either c_f or $c_m^{(k)}$ depending on the sign of $q_{fn}^{(k)}$. Using (5), additionally to the exchange terms in (2), we impose

$$\left.\begin{aligned} \rho(c_m^{(k)})\mathbf{q}_m\cdot\mathbf{n}^{(k)} &= Q_{fn}^{(k)} \\ \rho(c_m^{(k)})c_m^{(k)}\mathbf{q}_m\cdot\mathbf{n}^{(k)} + \rho(c_m^{(k)})\mathbf{D}_m\nabla c_m\cdot\mathbf{n}^{(k)} &= P_{fn}^{(k)} \end{aligned}\right\}, \qquad x \in \mathscr{S}^{(k)} \tag{7}$$

for $k = 1, 2$ that couple systems (1) and (2). The primary variables in this model are c_m, c_f, p_m and p_f. System (1–7) must be closed by boundary conditions for these variables on $\partial\mathcal{D}$ and initial conditions for c_m and c_f at $t = 0$.

3 Model problem settings

For our numerical tests, we choose and extension of the Henry problem [5, 13] — a two-dimensional model problem with one fracture, proposed in [4]: We consider $\mathcal{D} = [0, 2]\times[-1, 0]$ [m^2] with $\mathscr{S}$ touching its right "sea side" where the heavy salty water intrudes into the aquifer. The ends of $\mathscr{S}$ are at $(1, -0.7)$ and $(2, -0.5)$, see Fig. 1 (left). On the left, the recharge of fresh water is imposed: $c_m|_{x=0} = 0$, $\rho\mathbf{q}_m\cdot\mathbf{e}_x|_{x=0} = \hat{q}_{\text{in}}$, where $\mathbf{e}_x = (1, 0)^\top$, and $\hat{q}_{\text{in}}$ is a prescribed function of time, see below. On the right, we model the seawater intrusion: $c_{m,f}|_{x=2} = 1$, $p_{m,f}|_{x=2} = -\rho_1 g y$. On the top and the bottom of $\mathcal{D}$, no-flux boundary conditions are used. The flow and salt transport patterns for this problem are shown in Fig. 1 (right). The colour represents the mass fraction c_m, with dark red for $c_m = 1$ and dark blue for $c_m = 0$ ($c_m \in [0, 1]$). The lines are the streamlines of $\mathbf{q}_m$. In the left part of $\mathcal{D}$, the flow is induced by the pure water recharge. The salty water intruding through the lower part of the right boundary turns up and is flushed out through the upper part of the same side. In particular, the much more permeable fracture acts as a pathway for the strong washout. Due to this, the part of the domain below the fracture is almost separated from the upper part of the domain. This phenomenon depends on the aperture, porosity and permeability of the fracture.

In this paper, we set $\rho_{m,f}(c) = 10^3 + 25c$ $[kg/m^3]$, $\mu = 10^{-3}$ $[kg/m/s]$, $\mathbf{g} = (0, -9.8)^T$ $[m/s^2]$. In the fracture, $\phi_f = 0.7$ and $K_f = 1.019368\cdot 10^{-6}$ $[m^2]$ are deterministic. Besides that, we assume isotropic $\mathbf{K}_m = K_m\mathbf{I}$ with $K_m(\phi_m) = 1.5455\cdot 10^{-8}\phi_m^3/(1-\phi_m^2)$ $[m^2]$. We neglect the mechanical dispersion: $\mathbf{D}_m =$

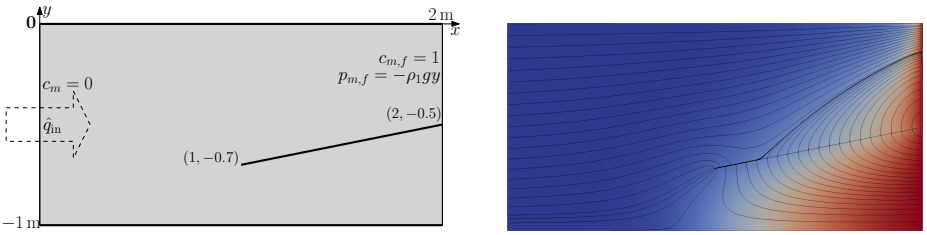

Fig. 1: (left) Scheme of the test problem; (right) flow streamlines (thin black lines) and the salt mass fraction field in $\mathcal{D}$. The dark red colour corresponds to $c_m = 1.0$, the dark blue to $c_m = 0$.

$\phi_m D_0 \mathbf{I}$, $D_f = \phi_f D_0$, where $D_0 = 18.8571 \cdot 10^{-6}$ $[m^2/s]$. Furthermore, we set $K_{fn} = K_m$ and $D_{fn} = \phi_m D_0$.

We consider uncertain porosity field ϕ_m, the fracture aperture ϵ, as well as the freshwater recharge intensity $\hat{q}_x$ (constant along the left boundary). Let $\xi_1(\omega), \xi_2(\omega), \xi_3(\omega) \in U[-1, 1]$ be three uniform RVs. The uncertain aperture of the fracture, the recharge, and the porosity are modeled as follows:

$$\epsilon(\xi_1) = 0.01 \cdot ((1 - 0.01) \cdot \xi_1 + (1 + 0.01))/2, \tag{8}$$

$$\hat{q}_{\text{in}}(t, \xi_3) = 3.3 \cdot 10^{-6} \cdot (1 + 0.1\xi_3)(1 + 0.1 \sin(\pi t/40)), \tag{9}$$

$$\phi_m(x, y, \xi_2) = 0.35 \cdot (1 + 0.02 \cdot (\xi_2 \cos(\pi x/2) + \xi_2 \sin(2\pi y)), \ (x, y) \in \mathcal{D}. \tag{10}$$

The QoI is the following time moment:

$$Q(\omega) = Q(\xi_1, \xi_2, \xi_3) := \min_t \{c_m(t, \mathbf{x}, \omega) \geq c^*\}, \tag{11}$$

where $c_m = c_m(t, \mathbf{x}, \omega)$ is the salt mass fraction at a fixed point $\mathbf{x} \in \mathcal{D}$, and c^* a specified critical value.

4 Numerical Methods

The initial system is numerically solved over the domain $\mathcal{D} \times [0, T]$, where $\mathcal{D}$ is discretized using an unstructured grid $\mathcal{D}_h$ composed of triangles and quadrilaterals. The characteristic mesh size on level ℓ is denoted by h_ℓ. To resolve the jump in the solution at $\mathscr{S}$, we apply a specialized technique, as detailed in [11]. The discretization in space is performed using a vertex-centered finite-volume scheme. We let n_ℓ represent the number of degrees of freedom on the grid. A regular refinement strategy is employed to construct the grid hierarchy, ensuring that $h_\ell = \mathcal{O}(n_\ell^{-1/d})$. In time, we use the implicit Euler method with a time step τ_ℓ. The total number of time steps is given by $r_\ell = T/\tau_\ell$.

We observed that after approximately $T = 6016$ seconds, the solution stabilizes and shows little change. Therefore, the experiment is conducted for $t \in [0, T]$. On the coarsest level we use $r_1 = 188$ time steps, yielding a time step

$\tau_1 = \frac{T}{r_1} = \frac{6016}{188} = 32$ seconds. For higher levels, $\ell = \{2, 3, 4, 5\}$, the number of time steps r_ℓ is $\{376, 752, 1504, 3008\}$, with the corresponding time step $\tau_\ell = \{16, 8, 4, 2\}$ seconds.

Due to the full upwind technique for the convective terms, the discretization error is of the first order w.r.t. h. Furthermore, the Euler method provides the same order w.r.t. τ. Thus, as $d = 2$, $\|c_m - c_{m,h,\tau}\|_2 = \mathcal{O}(h+\tau) = \mathcal{O}(n^{-1/2}+r^{-1})$, which is consistent with our numerical tests.

The implicit time-stepping scheme is unconditionally stable but requires solution of the large nonlinear algebraic system with n unknowns per time step by the Newton's method. The linear systems in the Newton iterations are solved using BiCGStab preconditioned with the GMG method (V-cycle) that involves the ILU_β-smoothers and Gaussian elimination as the coarse grid solver. The MLMC algorithm and the theory are described in [10]. We use GMG implemented in the ug4 toolbox [12, 14].

MLMC method. The MLMC method is an advanced variance reduction technique that leverages a hierarchy of discretization levels ($\ell = 0, \ldots, L$) to approximate the expected value of a QoI. The QoI at level ℓ is denoted by g_ℓ. Rather than relying solely on high-resolution simulations, MLMC combines multiple levels: coarser levels, which are computationally cheaper and provide rough estimates, and finer levels, which refine these estimates. The method achieves efficiency gains through a telescoping sum formulation, which systematically reduces variance across levels.

The MLMC method relies on three key components: 1) a sequence of increasingly fine discretizations in both space and time, 2) a hierarchical estimator that optimally balances accuracy and computational cost by distributing samples across levels, and 3) estimates of the weak and strong convergence rates, denoted by α and β, respectively.

The convergence rates α and β are determined by analyzing the decay of $\mathbb{E}[g_\ell - g_{\ell-1}]$ and $\text{Var}[g_\ell - g_{\ell-1}]$ as a function of ℓ. In the present study, for the quantity of interest (QoI) defined in (11) and evaluated at $\mathbf{x} = (1.1, -0.8)$, the estimated convergence rates are $\alpha \approx 1$ and $\beta \approx 1.7$. At another location, $\mathbf{x} = (1.2, -0.8)$, the rates are similar $\alpha \approx 1$ and $\beta \approx 1.65$. For further details how to use these rate, we refer to [9, 10] and the references therein.

Comparison of MC and MLMC methods. In Figure 2 (left), we show 50 random realizations of the mass fraction $c(t, \mathbf{x})$, computed at $\mathbf{x} = (1.1, -0.8)$, over time $t \in [0, 48\tau]$. Notably, there is substantial variability at the final time point, $t = 48\tau$.

Figure 2 (center) displays the probability density functions (pdfs) of the QoI computed at the point $\mathbf{x} = (1.1, -0.8)$ across different mesh levels labeled L1 (coarsest) through L5 (finest). The coarsest mesh (L1) contains 608 mesh points, and the next meshes $\{2368, 9344, 37120, 147968\}$ mesh points respectively. It is evident that curves L2 through L5 are nearly identical, whereas curve L1, corresponding to the coarsest mesh, diverges slightly, indicating reduced accuracy with coarser meshes. For instance, these plots say that in average after time

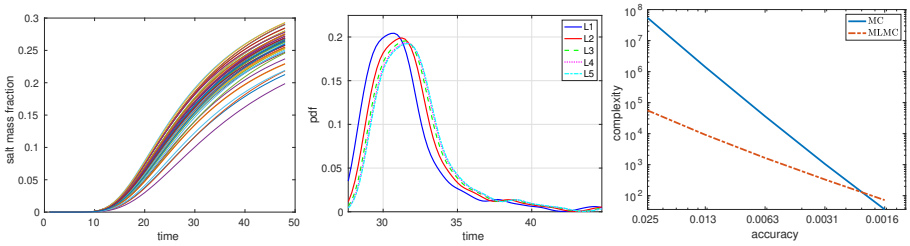

Fig. 2: (left) 50 random realizations of the mass fraction $c(t, \mathbf{x})$ over time t, where $t \in [0, 48\tau]$ at $\mathbf{x} = (1.1, -0.8)$; (center) pdfs of QoI, computed on different spatial and temporal scales (L1-L5); (right) Computational cost comparison of MC and MLMC methods against accuracy (scaled ε, horizontal axis) in log-log scale.

$t = 32\tau$, τ is a discrete time step, the mass fraction exceeds the threshold $c^* = 0.17$.

In Figure 2 (right), we compare the estimated computational costs for the MC method, shown by the blue solid line, and the Multi-Level Monte Carlo (MLMC) method, represented by the red dash-dot line. Both methods are used to compute $\mathbb{E}[g] = \mathbb{E}[Q](\mathbf{x}) := \mathbb{E}[Q(\omega, \mathbf{x})]$, with Q defined in (11). The horizontal axis indicates scaled accuracy ε. It is recommended to read the plot from right to left. The theoretical cost of the MC method is presented, as calculating it numerically is computationally prohibitive. The MLMC method's computational cost is given by $\mathcal{O}(\varepsilon^{-(2+\frac{3\cdot 1-1.7}{1})}) = \mathcal{O}(\varepsilon^{-3.3})$, which corresponds to the third case in the classical MLMC theorem [3, 1, 8]. We observe that the MLMC method outperforms MC for nearly all values of ε, particularly for small ε. The theoretical cost for MC is $\mathcal{O}(\varepsilon^{-2-\frac{\hat{d}\gamma}{\alpha}})$, with dimension $\hat{d} = 3$, $\gamma = 1$ (linear cost of the GMG method), and $\alpha = 1.08$. Hence, the theoretical cost for MC is $\mathcal{O}(\varepsilon^{-4.8})$. We calculated that achieving the smallest accuracy requires $L = 5$ levels, with the number of samples at each level being $(m_1, m_2, m_3, m_4, m_5) = (10463, 106, 20, 4, 1)$. This contrasts with the standard MC approach, where samples are only computed on the finest level.

Figure 3 shows similar pictures for the same QoI just computed at another point, namely, $\mathbf{x} = (1.2, -0.8)$. We see similar behavior and patterns in all three plots. The only difference is in the middle figure: The pdfs computed on different meshes are less similar to each other than on Figure 2. But the curves corresponding to the most finest meshes are very similar.

5 Discussion and Conclusion

In this study, we assessed the performance of the MLMC method by applying it to a Henry-like problem [5, 13], which models seawater intrusion into a 2D coastal aquifer with a fracture. This problem illustrates how freshwater recharge from the "land side" (see Fig. 1 (left)) counteracts the salinization caused by saline

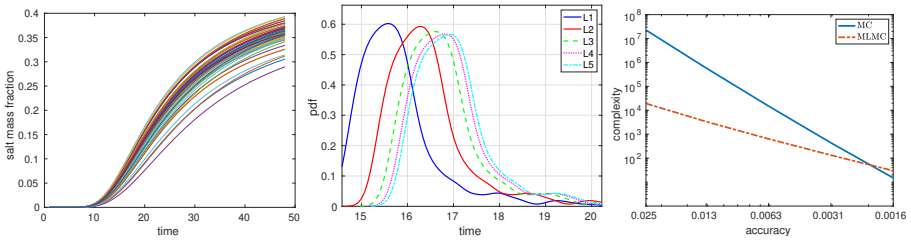

Fig. 3: (left) 50 random realizations of the mass fraction $c(t, \mathbf{x})$ over time t, where $t \in [0, 48\tau]$ at $\mathbf{x} = (1.2, -0.8)$; (center) pdfs of QoI, computed on different spatial and temporal scales (L1-L5); (right) Computational cost comparison of MC and MLMC methods against accuracy (scaled ε, horizontal axis) in log-log scale.

water intrusion from the "sea side", leading to an equilibrium in salt concentration over time.

To incorporate uncertainties in the system, several parameters were treated as random variables: the fracture width, porosity and permeability of the bulk medium, and the freshwater recharge rate from the land side. Porosity and permeability were modeled as correlated random fields, while the recharge rate was treated as a random periodic function, and the fracture width as a random variable. In total, three independent random variables were considered in the model.

The efficiency of the MLMC method was evaluated by computing the mean values of the earliest time at which the mass fraction exceeds a critical threshold.

The preliminary findings of this study highlight the significant potential of the MLMC method in reducing computational costs, with reductions of up to a factor of 1000 (see Fig. 2 and Fig. 3).

Preliminary experiments also underscore the critical importance of the choice of QoI. For smooth QoIs, such as integrals of the solution, the advantages of MLMC may be less pronounced. This is because integrals act as averaging operators, smoothing high-frequency fluctuations and reducing sensitivity to fine-scale features. As a result, such QoIs can often be accurately approximated using coarser meshes, which reduces the need for MLMC's multi-level refinement. Furthermore, the efficiency of MLMC is closely tied to both weak and strong convergence rates. Poor convergence can arise from various factors, including non-linearity in the problem, suboptimal discretization schemes, modeling errors, or numerical diffusion. These challenges emphasize the need for careful consideration of the problem's specific characteristics and the selection of appropriate numerical methods to ensure robustness and accuracy in the results.

Acknowledgments. For computer time of the presented numerical tests, this research used Shaheen II supercomputer managed by the Supercomputing Core Laboratory at King Abdullah University of Science & Technology (KAUST) in Thuwal, Saudi Arabia. This work was supported by the Alexander von Humboldt foundation.

Disclosure of Interests. The authors have no competing interests.

References

1. Collier, N., Haji-Ali, A.L., Nobile, F., von Schwerin, E., Tempone, R.: A continuation multilevel monte carlo algorithm. BIT Numerical Mathematics **55**(2), 399–432 (2015)
2. Dhal, L., Swain, S.: Understanding and modeling the process of seawater intrusion: a review, pp. 269–290 (01 2022). https://doi.org/10.1016/B978-0-12-823830-1.00009-2
3. Giles, M.B.: Multilevel Monte Carlo methods. Acta Numerica **24**, 259–328 (2015)
4. Grillo, A., Logashenko, D., Stichel, S., Wittum, G.: Simulation of density-driven flow in fractured porous media. Advances in Water Resources **33**(12), 1494–1507 (2010). https://doi.org/10.1016/j.advwatres.2010.08.004
5. Henry, H.R.: Effects of dispersion on salt encroachment in coastal aquifers, in 'seawater in coastal aquifers'. US Geological Survey, Water Supply Paper **1613**, C70–C80 (1964)
6. Litvinenko, A., Logashenko, D., Tempone, R., Wittum, G., Keyes, D.: Solution of the 3d density-driven groundwater flow problem with uncertain porosity and permeability. GEM - International Journal on Geomathematics **11**(1), 10 (2020). https://doi.org/10.1007/s13137-020-0147-1
7. Litvinenko, A., Logashenko, D., Tempone, R., Wittum, G., Keyes, D.: Propagation of uncertainties in density-driven flow. In: Bungartz, H.J., Garcke, J., Pflüger, D. (eds.) Sparse Grids and Applications — Munich 2018. pp. 101–126. Springer, Cham (2021). https://doi.org/10.1007/978-3-030-81362-8_5
8. Litvinenko, A., Yucel, A.C., Bagci, H., Oppelstrup, J., Michielssen, E., Tempone, R.: Computation of electromagnetic fields scattered from objects with uncertain shapes using multilevel monte carlo method. IEEE Journal on Multiscale and Multiphysics Computational Techniques **4**, 37–50 (2019). https://doi.org/10.1109/JMMCT.2019.2897490
9. Logashenko, D., Litvinenko, A., Tempone, R., Vasilyeva, E., Wittum, G.: Uncertainty quantification in the henry problem using the multilevel monte carlo method. Journal of Computational Physics **503**, 112854 (2024). https://doi.org/10.1016/j.jcp.2024.112854
10. Logashenko, D., Litvinenko, A., Tempone, R., Wittum, G.: Estimation of uncertainties in the density driven flow in fractured porous media using mlmc. Engineering with Computers (2024). https://doi.org/10.1007/s00366-024-02089-6
11. Reiter, S., Logashenko, D., Stichel, S., Wittum, G., Grillo, A.: Models and simulations of variable-density flow in fractured porous media. International Journal of Computational Science and Engineering **9**(5-6), 416–432 (2014). https://doi.org/10.1504/IJCSE.2014.064527
12. Reiter, S., Vogel, A., Heppner, I., Rupp, M., Wittum, G.: A massively parallel geometric multigrid solver on hierarchically distributed grids. Computing and Visualization in Science **16**(4), 151–164 (August 2013). https://doi.org/10.1007/s00791-014-0231-x
13. Simpson, M.J., Clement, T.P.: Improving the worthiness of the Henry problem as a benchmark for density-dependent groundwater flow models. Water Resources Research **40**(1), W01504 (Jan 2004). https://doi.org/10.1029/2003WR002199
14. Vogel, A., Reiter, S., Rupp, M., Nägel, A., Wittum, G.: Ug 4: A novel flexible software system for simulating pde based models on high performance computers. Computing and Visualization in Science **16**(4), 165–179 (August 2013). https://doi.org/10.1007/s00791-014-0232-9